

GaN/Fe core/shell nanowires for nonvolatile spintronics on Si

Cunxu Gao,* Rouin Farshchi, Claudia Roder, Pinar Dogan, and Oliver Brandt

Paul-Drude-Institut für Festkörperelektronik, Hausvogteiplatz 5–7, D-10117 Berlin, Germany

(Received 25 March 2011; published 29 June 2011)

We explore the relationship between the structural and magnetic properties of GaN/Fe core/shell nanowires grown epitaxially on Si substrates. The magnetic properties are consistent with the coexistence of two magnetic contributions: a ferromagnetic response from the single-crystalline Fe particles formed at the nanowire tips, and a superparamagnetic response originating from the granular Fe clusters grown on the nanowire sidewalls, giving them a corn-cob-like morphology. We show that our interpretation of the origin of the magnetic behavior can be confirmed by the viscous decay of magnetic remanence in the nanowires. Ferromagnetic remanence is observed both parallel and perpendicular to the nanowire axis, making such structures appealing as high-density nonvolatile spintronic components on Si.

DOI: [10.1103/PhysRevB.83.245323](https://doi.org/10.1103/PhysRevB.83.245323)

PACS number(s): 61.46.Km, 68.37.–d, 75.50.–y, 81.15.Hi

I. INTRODUCTION

Core/shell nanowires (NWs) have captivated the imagination of many researchers over the past decade due to their novel functionalities over a range of potential applications.^{1–5} In particular, high-quality III-V semiconductor (SC) core/shell structures of GaAs, GaP, and GaN NWs on Si substrates are finally bridging the lattice incompatibility gap between Si electronics and III-V optical components that has plagued thin films for decades,⁶ hence allowing for III-V NW light-emitting diodes (LEDs)⁷ and lasers^{8,9} to be grown on Si substrates.

The introduction of a ferromagnetic (FM) component as the shell adds even more versatility to core/shell NWs.^{10–12} Injection of spin-polarized electrons from FMs into SCs and their subsequent manipulation in gated structures or conversion into circularly polarized light in spin-LEDs and spin vertical-cavity surface-emitting lasers (VCSELs) are active research areas in the field of SC spintronics,¹³ which aims to harness the spin information of electrons. Synthesis of such structures in NW form is advantageous for the realization of high-density memory elements, directional sources of circularly polarized light that can operate in magnetic remanence, and functional multilayer architectures such as spin-torque devices that cannot be realized as thin films in a bottom-up approach. A GaN core paired with an Fe shell is of particular interest, since the Fe/GaN interface has been shown to be thermodynamically stable.¹⁴ Moreover, epitaxial GaN films have been grown on Fe substrates,¹⁵ representing one of the rare exceptions of a successful SC-on-metal epitaxy, potentially allowing for FM/SC/FM heterostructure NWs. Here, we synthesize GaN/Fe core/shell NWs on a Si substrate by molecular beam epitaxy (MBE) and find that the structural properties of the Fe shell result in the coexistence of FM and superparamagnetic (SP) contributions, in strong contrast to Fe/GaN thin-film heterostructures. Furthermore, the NWs exhibit a nonvanishing remanence in both parallel and perpendicular field configurations, making them attractive for nonvolatile spintronic applications.

II. EXPERIMENTAL

The epitaxial growth of the GaN/Fe core/shell NWs was performed in a custom-built plasma-assisted MBE system

equipped with solid-source effusion cells for Ga and Fe. Active nitrogen was provided by a radiofrequency N₂ plasma source. Nucleation and growth were monitored *in situ* by reflection high-energy electron diffraction (RHEED). GaN NWs were grown directly on Si(111) 2'' wafers under N-rich conditions (N/Ga = 3) at a substrate temperature of 800 °C. Directly after growth of the GaN NWs, the substrate was cooled down to 350 °C and Fe deposition was initiated with an Fe flux of 1.7×10^{13} atoms/cm²s, while keeping the chamber pressure at the low 10^{–9} mbar range. Both during GaN and Fe growth, the substrates were continuously rotated to ensure homogeneous conditions across the wafer. To assess the NW morphology, the samples were cleaved into smaller pieces for investigation by scanning electron microscopy (SEM) and transmission electron microscopy (TEM), the latter through the standard mechanical thinning and ion-milling processes. A reference sample consisting of an Fe film with a thickness of 24 nm was grown at a substrate temperature of 350 °C on a GaN layer. Finally, the magnetic properties of the NWs and the reference sample were measured in a superconducting quantum interference device magnetometer (SQUID). All magnetization data presented here are corrected for the diamagnetic background of the substrate.

III. RESULTS AND DISCUSSION

We focus on two sets of samples, each comprised of a sample with low and high Fe coverage and essentially differing in the length of the NWs. Figure 1 depicts SEM images taken in top-view of samples S1–S4. In all cases, a high-density NW array, with an estimated density of more than 10¹⁰ NWs/cm², is observed. The diameter distributions are broad with average values increasing with the growth times of the GaN NWs as well as the Fe deposition (see below for quantitative results). Side-view SEM images of samples S1–S4 are shown in Fig. 2 and reveal that the NWs are vertically aligned and exhibit an average height solely determined by the growth time of the GaN NWs. The presence of Fe becomes clearly evident in images with higher magnification, as displayed in Fig. 3 for samples S1–S4. While bare GaN NWs exhibit atomically smooth (10 $\bar{1}$ 0) side and (0001) top facets, the Fe deposition results in a corn-cob-like morphology of the NWs side facets and pronounced hats

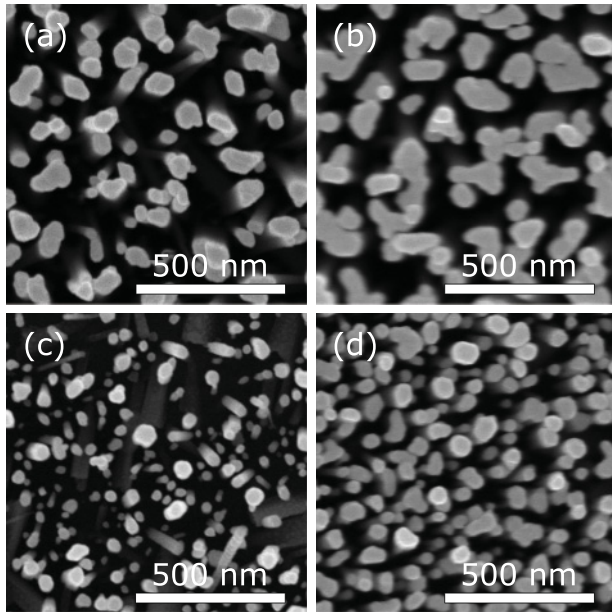


FIG. 1. Top-view SEM images of sample (a) S1, (b) S2, (c) S3, and (d) S4, respectively, acquired at low magnification, as elaborated by the scale bars.

on top. Table I summarizes the structural parameters of samples S1–S4 as obtained by the micrographs displayed in Figs. 1–3.

To investigate this peculiar morphology of the GaN/Fe NWs in more detail, isolated NWs were investigated by TEM. The plan-view micrograph shown in Fig. 4(a) reveals a shell of granular Fe clusters enclosing a hexagonal GaN core. The Fe clusters on the sidewalls appear to be embedded in an amorphous matrix, which presumably consists of Fe_xO_y . The cross-sectional TEM image shown in Fig. 4(b) displays the Fe clusters giving rise to the corncob appearance of the NWs. These clusters are crystalline, but a determination of their orientation has proven to be very difficult due to their nanoscopic size. The larger Fe particle formed on the tip of the NW is particularly visible in the high-resolution micrograph shown in Fig. 4(c). This particle is single-crystalline, as clearly seen in the lattice image displayed in Fig. 4(d).

The orientation relationship (OR) between the Fe crystallite and the GaN NW as deduced from our TEM investigations is known as the Pitsch-Schrader (PS) OR and is defined by $\text{Fe}(110)\langle 001 \rangle \parallel \text{GaN}(0001)\langle 11\bar{2}0 \rangle$,¹⁶ as displayed by the ball-and-stick model presented in Fig. 4(e). The PS OR is not unique but has three symmetry equivalents. In fact, for planar Fe films on GaN(0001), all these symmetry equivalents are observed to coexist, and the Fe film is consequently found to consist of domains rotated with respect to each other by 120° .^{14,17–20} The size of these domains depends on temperature, and reaches values well above 100 nm for the current growth temperature of 350°C . The small diameters realized in our NW ensembles thus afford only a single structural domain of Fe on the GaN NW tip. Okamoto *et al.*¹⁵ have demonstrated that GaN(0001) films grow epitaxially on Fe(110) substrates. Similar to our studies on Fe/GaN,¹⁴ they found that the GaN/Fe heterointerface remains abrupt even after annealing at 700°C . These results suggest the possibility

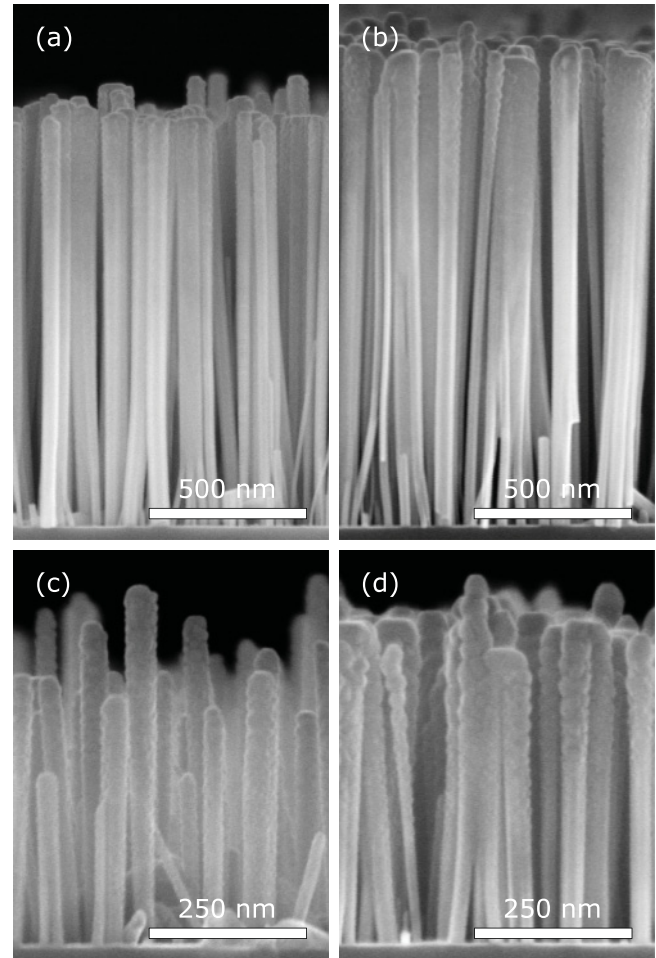


FIG. 2. Side-view SEM images of sample (a) S1, (b) S2, (c) S3, and (d) S4, respectively, acquired at low magnification, as elaborated by the scale bars.

to fabricate GaN/Fe/GaN axial heterostructure NWs, allowing for additional flexibility in device design.

The morphology of the GaN/Fe NWs under investigation has interesting consequences on their magnetic properties as measured by SQUID. It can be seen from the magnetic hysteresis loops recorded at 10 K in Figs. 5(a) and 5(b) that the NWs display nonvanishing remanence for both the parallel and perpendicular field configurations, in contrast to planar Fe films, which normally display a magnetic hard axis in the out-of-plane direction and therefore exhibit zero remanence in this configuration.²¹ Furthermore, the NW hysteresis loops reveal a complex magnetic-field dependence. The peculiar shapes of the curves have been figuratively categorized by Tauxe *et al.*²² into *wasp-waisted* and *pot-bellied* loops. We observe wasp-waisted (pot-bellied) loops with the magnetic field applied parallel (perpendicular) to the NW axis, as shown in Figs. 5(a) and 5(b) for samples S1 and S2, respectively. It has been shown by Tauxe *et al.*²² that either of these shapes can arise due to the coexistence of single-domain FM and SP phases. In our case, the former presumably arises from the single-crystal Fe hats on top of the NWs, while the latter contribution is likely to originate from the small Fe clusters nucleated on the side facets.

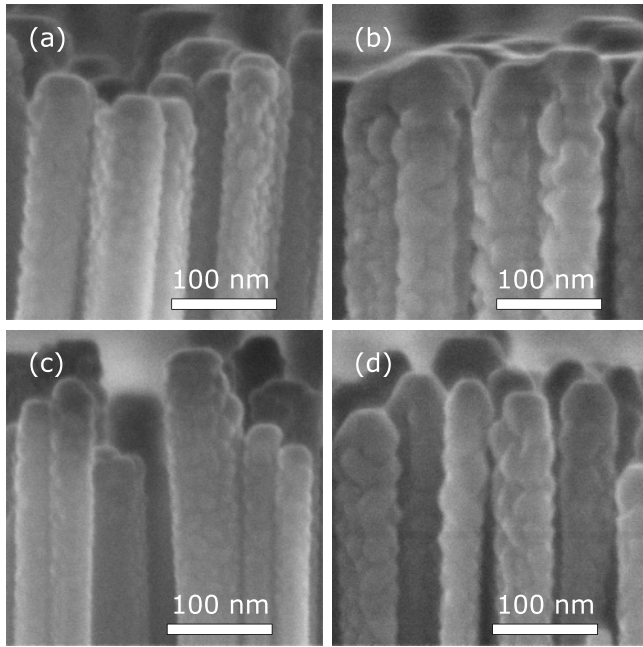


FIG. 3. Side-view SEM images of sample (a) S1, (b) S2, (c) S3, and (d) S4, respectively, acquired at high magnification, as elaborated by the scale bars.

Tauxe *et al.* further argued that wasp-waisting (pot-bellying) is favored when the magnetization of the SP phase has a steep (gentle) field dependence, which in the present case occurs in measurements taken parallel (perpendicular) to the NW axis.

Evidence for the existence of an SP phase in both S1 and S2 NWs can be found from the temperature dependence of the coercive field, as shown in Fig. 5(c). The coercive field (H_c) of the ferromagnetic film grown on GaN exhibits a linear temperature dependence, as shown with black triangles. An SP contribution is expected to manifest itself as a superlinear increase of coercivity upon cooling below the blocking temperature.^{23–25} The curves for the NWs clearly exhibit this expected increase for temperatures below ~ 100 K, where the temperature dependence is in reasonable agreement with measurements on samples containing SP particles by Vavassori *et al.*²³ This temperature dependence is generally stronger than the $T^{3/4}$ or $T^{1/2}$ dependencies expected for noninteracting SP particles. According to Vavassori *et al.*,²³ this behavior can be attributed to the nonuniformity of particle sizes. Comparison of the curves for S1 and S2 in Fig. 5(c) shows that the magnetic coercivity generally increases with Fe deposition time. This

TABLE I. Summary of the structural parameters of the samples investigated in this work. Given is the length l as well as the mean equivalent disk diameter d of the NWs and the nominal amount of Fe deposited in terms of the equivalent layer thickness t .

Sample	l (μm)	d (nm)	t (nm)
S1	1.3	56	9.8
S2	1.5	130	25.2
S3	0.5	36	7.2
S4	0.5	90	24.0

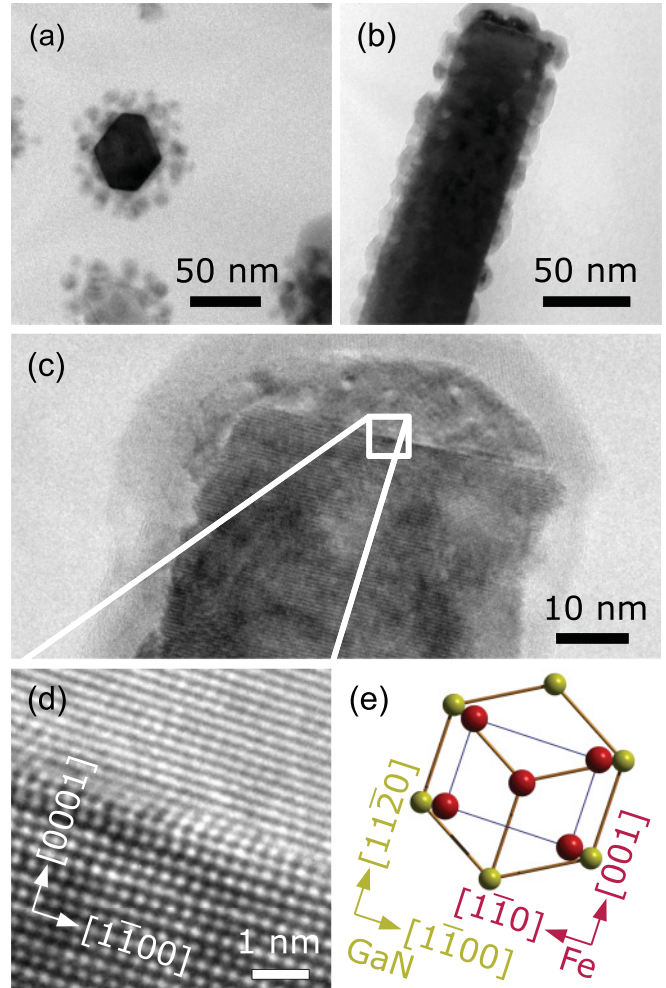


FIG. 4. (Color online) (a) Plan-view and (b) cross-sectional TEM images of sample S3. (c) and (d) Cross-sectional high-resolution TEM images of sample S4. (e) Schematic ball-and-stick model showing the PS OR for Fe (dark) on the top Ga layer (light) of GaN(0001).

fact may be due to a larger distribution of grain sizes in the case of the S2 NWs, and provides the opportunity to tune the magnetic coercivity by adjusting the Fe deposition time.

Further evidence for the coexistence of SP and FM contributions can be obtained from Fig. 5(d), where we show the temperature dependence of the normalized remanent magnetization of our samples. For these measurements, the samples are first cooled to 10 K in zero magnetic field (zero-field cooled), then magnetized at 50 kOe, followed by reduction of the applied field to zero. For the case of the Fe film on GaN shown by black triangles, the remanent magnetization decreases only very slightly (4.5%) up to 350 K. The NWs, on the other hand, exhibit a strong initial reduction in remanent magnetization, followed by a more steady reduction that persists above room temperature. Such a strong reduction of remanent magnetization with temperature is not expected to occur in purely ferromagnetic Fe, and is attributed to an SP response. The stronger reduction from 10 K to 350 K for S1 (70%) compared to S2 (50%) is consistent with a larger volume fraction of the SP phase in S1 compared to S2.

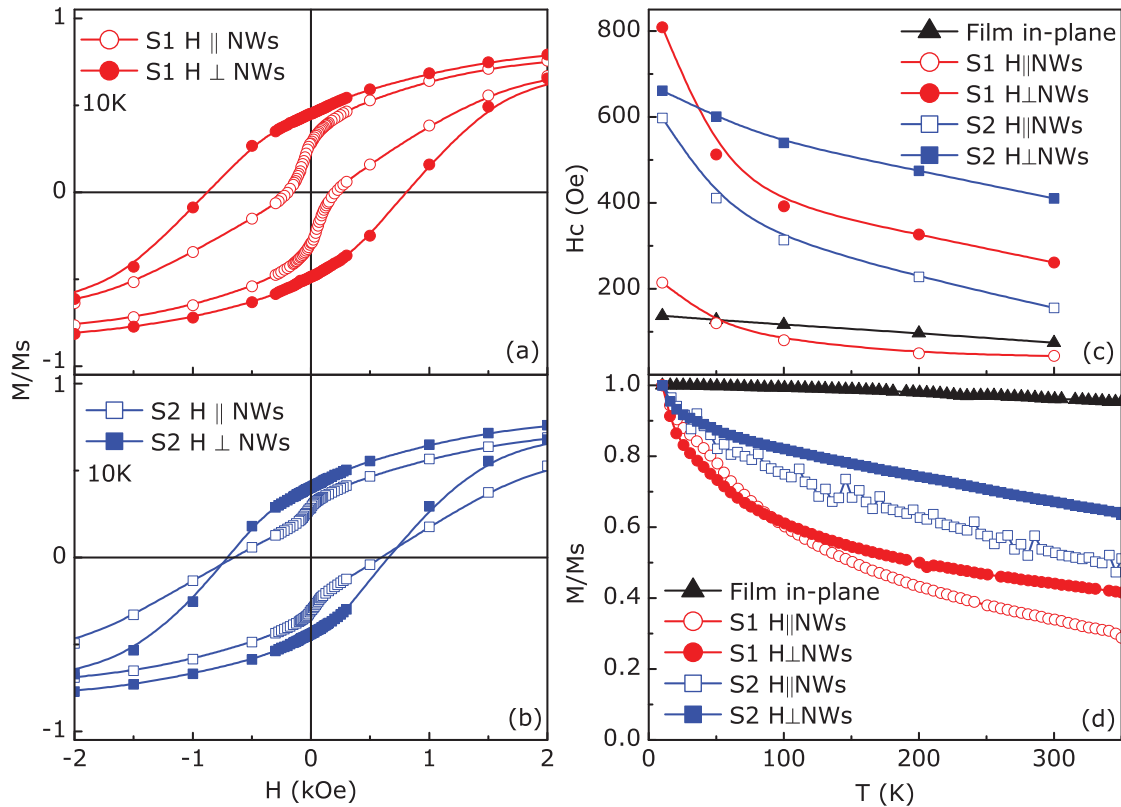


FIG. 5. (Color online) Magnetic hysteresis loops of the GaN/Fe core/shell NW arrays of sample (a) S1 and (b) S2 obtained at 10 K with the magnetic field parallel and perpendicular to their long axis, i.e., the GaN[0001] direction. (c) Coercive field vs temperature for samples S1 and S2 in comparison to that of an Fe film on GaN. The solid lines are guides to the eyes. (d) Temperature dependence of the magnetization of the NW arrays for samples S1 and S2 in comparison to that of an Fe film on GaN.

The reduction in remanent magnetization with temperature is stronger with field applied parallel to the NWs for both S1 and S2, presumably reflecting the anisotropy of the SP phase.

An interesting ramification of an SP phase is the fingerprint observed in isothermal remanent magnetization measurements (IRM), namely the viscous decay of the remanent magnetization with time.^{26–28} According to Worm *et al.*,²⁷ single-domain particles of a ferromagnetic phase are stable carriers of magnetic remanence when they are of sufficient size, while SP particles well below the threshold size preserve no remanence at all. However, particles just around the threshold size do not have a stable magnetization, resulting in a slow decay of the remanent magnetization of the particle ensemble with time. For our IRM experiments, the sample is first cooled to 10 K in zero magnetic field and magnetized at 10 K at a field of 20 kOe for 5 min, followed by a removal of the field and measurement of the remanent magnetization, as shown in Fig. 6. For the case of the Fe film on GaN, shown by black triangles, the remanent magnetization is maintained over the experimental durations considered here. This is not the case for samples S1 and S2, shown by red circles and blue squares, respectively, for which a near-logarithmic decay of about 1%–3% is observed, which directly reveals the coexistence of the FM and SP phases. The stronger decay for sample S1 compared to sample S2 reflects the larger fractional volume of SP particles in sample S1.

IV. CONCLUSION

The remarkably high crystalline quality and interface perfection of the single-domain FM Fe particles grown on top of the GaN NWs may open new possibilities for

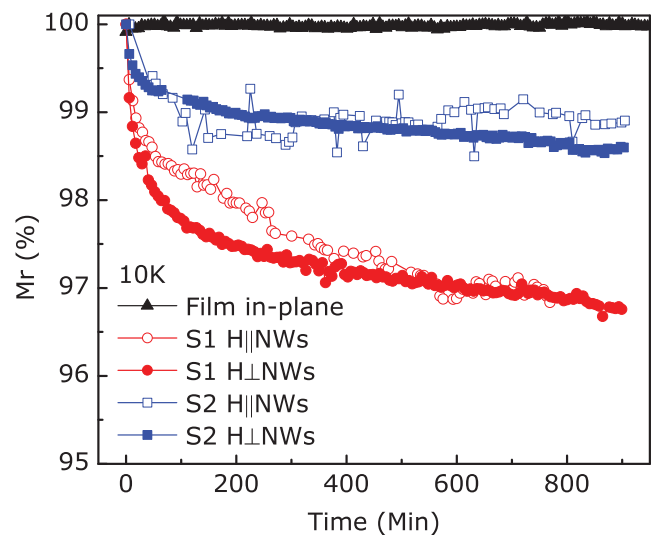


FIG. 6. (Color online) Isothermal remanent magnetization of the NW arrays for samples S1 and S2 obtained at 10 K in contrast to that of an Fe film on GaN.

spin-based FM/SC nanowire research. Such high-quality interfaces are imperative for efficient injection of spins into the SC, which serves as the starting point for the operation of spin-LEDs and spin-valve devices. The occurrence of magnetic remanence both parallel and perpendicular to the NW axis would allow for operation of such devices in the absence of a magnetic field. The influence of the SP phase forming on the NW sidewall on the performance of such devices remains to be seen. Nonetheless, longer Fe deposition times should lead to larger Fe clusters on the NW sidewall, with the grains eventually exceeding the SP threshold and transitioning to the FM phase. Incorporating techniques for GaN nanowire growth on prepatterned Si substrates²⁹

followed by appropriate electrical contact³⁰ can lead to the realization of regularly arrayed nanowire spin-LEDs on Si, where the nanowire diameters will depend on the pattern dimensions.

ACKNOWLEDGMENTS

We thank Jens Herfort for a critical reading of the manuscript, Anne-Kathrin Bluhm for SEM, and Hans-Peter Schönherr for constant maintenance of the MBE system used for the present work. We are indebted to Lutz Geelhaar for continuous encouragement and support. R.F. acknowledges support from the Alexander von Humboldt Foundation.

*gaocunx@pdi-berlin.de

¹L. J. Lauhon, M. S. Gudiksen, D. Wang, and C. M. Lieber, *Nature (London)* **420**, 57 (2002).

²D. H. Zhang, Z. Q. Liu, S. Han, C. Li, B. Lei, M. P. Stewart, J. M. Tour, and C. W. Zhou, *Nano Lett.* **4**, 2151 (2004).

³J. Xiang, W. Lu, Y. J. Hu, Y. Wu, H. Yan, and C. M. Lieber, *Nature (London)* **441**, 489 (2006).

⁴J. A. Czaban, D. A. Thompson, and R. R. LaPierre, *Nano Lett.* **9**, 148 (2009).

⁵Y. T. Chong, D. Görlitz, S. Martens, M. Y. E. Yau, S. Allende, J. Bachmann, and K. Nielsch, *Adv. Mater.* **22**, 2435 (2010).

⁶T. Mårtensson, C. P. T. Svensson, B. A. Wacaser, M. W. Larsson, W. Seifert, K. Deppert, A. Gustafsson, L. R. Wallenberg, and L. Samuelson, *Nano Lett.* **4**, 1987 (2004).

⁷F. Qian, S. Gradeak, Y. Li, C. Y. Wen, and C. M. Lieber, *Nano Lett.* **5**, 2287 (2005).

⁸B. Hua, J. Motohisa, Y. Kobayashi, S. Hara, and T. Fukui, *Nano Lett.* **9**, 112 (2009).

⁹J. C. Johnson, H. J. Choi, K. P. Knutsen, R. D. Schaller, P. D. Yang, and R. J. Saykally, *Nat. Mater.* **1**, 106 (2002).

¹⁰A. Rudolph, M. Soda, M. Kiessling, T. Wojtowicz, D. Schuh, W. Wegscheider, J. Zweg, C. Back, and E. Reiger, *Nano Lett.* **9**, 3860 (2009).

¹¹M. Hilse, Y. Takagaki, J. Herfort, M. Ramsteiner, C. Herrmann, S. Breuer, L. Geelhaar, and H. Riechert, *Appl. Phys. Lett.* **95**, 133126 (2009).

¹²N. S. Dellas, J. Liang, B. J. Cooley, N. Samarth, and S. E. Mohny, *Appl. Phys. Lett.* **97**, 072505 (2010).

¹³S. A. Wolf, D. D. Awschalom, R. A. Buhrman, J. M. Daughton, S. von Molnár, M. L. Roukes, A. Y. Chtchelkanova, and D. M. Treger, *Science* **294**, 1488 (2001).

¹⁴C. X. Gao, O. Brandt, H.-P. Schönherr, U. Jahn, J. Herfort, and B. Jenichen, *Appl. Phys. Lett.* **95**, 111906 (2009).

¹⁵K. Okamoto, S. Inoue, N. Matsuki, T. W. Kim, J. Ohta, M. Oshima, H. Fujioka, and A. Ishii, *Appl. Phys. Lett.* **93**, 251906 (2008).

¹⁶W. Pitsch and A. Schrader, *Arch. Eisenhüttenwes.* **29**, 715 (1958).

¹⁷R. Meijers, R. Calarco, N. Kaluza, H. Hardtdegen, M. Ahe, H. L. Bay, H. Lüth, M. Buchmeier, and D. E. Bürgler, *J. Cryst. Growth* **283**, 500 (2005).

¹⁸C. X. Gao, H.-P. Schönherr, and O. Brandt, *Appl. Phys. Lett.* **97**, 031906 (2010).

¹⁹C. X. Gao, O. Brandt, S. C. Erwin, J. Lähnemann, U. Jahn, B. Jenichen, and H.-P. Schönherr, *Phys. Rev. B* **82**, 125415 (2010).

²⁰C. X. Gao, O. Brandt, J. Lähnemann, J. Herfort, H.-P. Schönherr, U. Jahn, and B. Jenichen, *J. Cryst. Growth* **323**, 359 (2011).

²¹R. C. O'Handley, *Modern Magnetic Materials: Principles and Applications* (Wiley, New York, 2000), p. 314.

²²L. Tauxe, T. A. T. Mullender, and T. Pick, *J. Geophys. Res.* **101**, 571 (1996).

²³P. Vavassori, E. Angeli, D. Bisero, F. Spizzo, and F. Ronconi, *Appl. Phys. Lett.* **79**, 2225 (2001).

²⁴C. P. Bean and J. D. Livingston, *J. Appl. Phys.* **30**, S120 (1959).

²⁵J. García-Otero, A. J. García-Bastida, and J. Rivas, *J. Magn. Magn. Mater.* **189**, 377 (1998).

²⁶T. Pick and L. Tauxe, *J. Geophys. Res.* **98**, 17949 (1993).

²⁷H. U. Worm, *Geophys. Res. Lett.* **26**, 2557 (1999).

²⁸T. A. Machac, C. W. Zanner, and C. E. Geiss, *Geophys. J. Int.* **169**, 483 (2007).

²⁹H. Sekiguchi, K. Kishino, and A. Kikuchi, *Appl. Phys. Express* **1**, 124002 (2008).

³⁰A. Kikuchi, M. Kawai, M. Tada, and K. Kishino, *Jpn. J. Appl. Phys.* **43**, L1524 (2004).